Universality of non-Ohmic shunt leakage in thin-film solar cells

Cite as: J. Appl. Phys. **108**, 124509 (2010); https://doi.org/10.1063/1.3518509
Submitted: 18 August 2010 . Accepted: 25 October 2010 . Published Online: 28 December 2010

S. Dongaonkar, J. D. Servaites, G. M. Ford, S. Loser, J. Moore, R. M. Gelfand, H. Mohseni, H. W. Hillhouse, R. Agrawal, M. A. Ratner, T. J. Marks, M. S. Lundstrom, M. A. Alam, et al.

Universality of non-Ohmic shunt leakage in thin-film solar cells

S. Dongaonkar,[1,a)] J. D. Servaites,[2] G. M. Ford,[3] S. Loser,[4] J. Moore,[1] R. M. Gelfand,[5] H. Mohseni,[5] H. W. Hillhouse,[3] R. Agrawal,[3] M. A. Ratner,[2,4,6] T. J. Marks,[2,4,6] M. S. Lundstrom,[1] and M. A. Alam[1,a)]

[1]*School of Electrical and Computer Engineering, Purdue University, West Lafayette, Indiana 47907, USA*
[2]*Department of Materials Science and Engineering, Northwestern University, Evanston, Illinois 60208, USA*
[3]*School of Chemical Engineering, Purdue University, West Lafayette, Indiana 47907, USA*
[4]*Department of Chemistry, Northwestern University, Evanston, Illinois 60208, USA*
[5]*Department of Electrical Engineering and Computer Science, Northwestern University, Evanston, Illinois 60208, USA*
[6]*The Argonne-Northwestern Solar Energy Research Center, Northwestern University, Evanston, Illinois 60208, USA*

(Received 18 August 2010; accepted 25 October 2010; published online 28 December 2010)

We compare the dark current-voltage (IV) characteristics of three different thin-film solar cell types: hydrogenated amorphous silicon (a-Si:H) p-i-n cells, organic bulk heterojunction (BHJ) cells, and $Cu(In,Ga)Se_2$ (CIGS) cells. All three device types exhibit a significant shunt leakage current at low forward bias ($V < \sim 0.4$) and reverse bias, which cannot be explained by the classical solar cell diode model. This parasitic shunt current exhibits non-Ohmic behavior, as opposed to the traditional constant shunt resistance model for photovoltaics. We show here that this shunt leakage (I_{sh}), across all three solar cell types considered, is characterized by the following common phenomenological features: (a) voltage symmetry about $V=0$, (b) nonlinear (power law) voltage dependence, and (c) extremely weak temperature dependence. Based on this analysis, we provide a simple method of subtracting this shunt current component from the measured data and discuss its implications on dark IV parameter extraction. We propose a space charge limited (SCL) current model for capturing all these features of the shunt leakage in a consistent framework and discuss possible physical origin of the parasitic paths responsible for this shunt current mechanism. © *2010 American Institute of Physics*. [doi:10.1063/1.3518509]

I. INTRODUCTION

Thin-film photovoltaic technologies are considered promising alternatives to conventional crystalline solar cells due to their significantly lower manufacturing and installation costs, materials versatility, and mechanical flexibility.[1–3] Consequently, a wide variety of these technologies, including amorphous and microcrystalline silicon (a-Si:H/μc-Si:H),[4] cadmium telluride (CdTe), copper indium gallium diselenide (CIGS),[5] and organic photovoltaics (OPVs),[6] are being developed and commercialized. These developments have necessitated a better understanding of thin film solar cell device physics, including important module performance variability issues. Such performance variability not only affects the yield in production, but also dictates what proportion of the single cell efficiency is ultimately translated into module efficiency.[5]

One such key issue affecting performance consistency for large area thin-film solar cells is an excess variable dark leakage current at low biases, commonly referred to as shunt leakage current (I_{sh}).[7–11] As shown in the schematic of Fig. 1(a), when this shunt leakage is sufficiently high, it can reduce the fill factor significantly, in turn adversely affecting the cell efficiency. Also, the magnitude of this leakage current is known to vary significantly and unpredictably from one cell to the other, even when the cells are fabricated under nominally identical conditions.[7,8,12] This variation in shunt leakage magnitude introduces another problem at the module level, where many identical cells must be connected in series to increase the output voltage. However, the variation in shunt current magnitude from cell to cell makes it difficult to predict the final panel output characteristics. This directly affects the panel yield which is becoming increasingly important as more thin film technologies are being developed and manufactured. Therefore, to address the problems introduced by this leakage current, it is crucial to understand the underlying factors affecting its magnitude and variability.

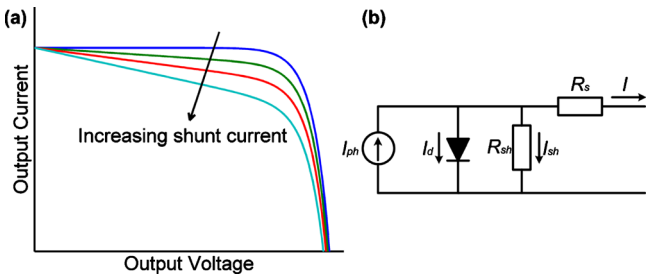

FIG. 1. (Color online) (a) Schematic showing the effect of increasing shunt leakage current on the output characteristics of the solar cell, obtained from the standard equivalent circuit picture. (b) Commonly used equivalent circuit model for solar cells, where photocurrent is represented as an ideal current source I_{ph}, the exponential device dark current as a diode current I_d, with a series resistance R_s. The shunt leakage I_{sh} is often assumed Ohmic, and represented by a parallel shunt resistance R_{sh}

[a)]Electronic addresses: sourabh@purdue.edu and alam@purdue.edu.

Shunt leakage currents have been discussed widely in literature for a range of different thin-film solar cell types, and a variety of explanations and models have been proposed. In terms of the electrical characteristics, shunt currents have been typically considered to be Ohmic in nature.[13–17] In the equivalent circuit picture, this is typically represented by a parallel resistance [Fig. 1(b)]. This simplified model allows us to write the output current I in terms of output voltage V as follows:

$$I = I_{ph} - I_{\text{dark}} = I_{ph} - [I_{sh} + I_d]$$

$$= I_{ph} - \overbrace{\left[\underbrace{\frac{V - IR_s}{R_{sh}}}_{I_{sh}} + \underbrace{I_0\left(e^{\frac{q(V-IR_s)}{nk_BT}} - 1\right)}_{I_d}\right]}^{I_{\text{dark}}}. \quad (1)$$

Here I_{ph} is the photocurrent, I_{dark} is the net dark current, R_s is the series resistance, I_0 is the reverse saturation current density, n is the diode ideality factor, k_B is Boltzmann's constant, and T is temperature. In this equivalent circuit picture, the shunt current (I_{sh}, through the parallel resistance R_{sh}) and the exponential diode current (I_d) account for the net dark current (I_{dark}) However, this picture has been shown to be incomplete since shunt leakage currents are known to exhibit a nonlinear dependence on the applied voltage.[8,9,13,18,19] Some equivalent circuits incorporating a parasitic weak diode have also been proposed to account for these nonlinear shunts.[19–21] However, these macroscopic, circuit level models cannot account for the microscopic nature of shunt paths.

The physical origin of shunt conduction paths have also been explored in the literature. For a-Si:H p-i-n solar cells, this shunt leakage has been attributed to lateral drift currents[14] and nonuniformities distributed across the surface.[22] The role of microscopic pinholes that might form in the active layer during film deposition has also been explored.[13] Experimental work showing the involvement of Al diffusion into the n layers has also been reported.[23] In the case of CIGS cells, one also finds disparate explanations in the literature for this shunt leakage phenomenon, including excess Cu content leading to conduction at grain boundaries or nanoscale phase segregation,[7] and pinholes requiring the use of a i-ZnO buffer layer.[24]

It is apparent from the discussion above that while the shunt leakage problem has been observed in all thin film PV technologies, it has been only discussed in isolated contexts. Therefore, there is a lack of coherent understanding of this phenomenon within a common theoretical framework. The analysis of shunt leakage phenomena is hampered, in part, because most models of the dark current typically focus on the forward bias current at one temperature only.[12,14,20,25] A detailed characterization of the shunt current, considering the entire voltage range at different temperatures, is usually not performed. Moreover, the picture of shunt leakage has been fragmented because the nature of shunt current has been assumed to be unique for solar cell technologies. In this article we will be addressing these issues to establish the universal features of shunt leakage current.

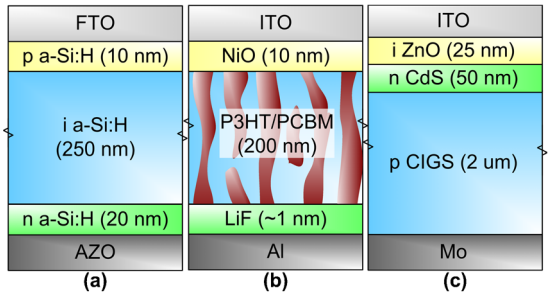

FIG. 2. (Color online) Schematics showing the ideal device structures and layer thicknesses of the three solar cell technologies considered here: (a) a-Si:H p-i-n solar cell, (b) P3HT:PCBM OPV, and (c) CIGS solar cell.

We begin by briefly describing the cell fabrication methods in Sec. II A, followed by a description of the simulation tools and methods in Sec. II B. In Sec. III, we present a thorough dark IV characterization of the three solar cell types (a-Si:H, OPV, and CIGS), over ~100 K temperature range. We find that regardless of thin-film solar cell type, the electrical characteristics of the shunt leakage are universal. Next, in Sec. IV we provide a simple subtraction scheme to remove the shunt component from measured forward current, and discuss the implication for parameter extraction. In Sec. V A, we propose a phenomenological space charge limited (SCL) current model to explain the universal shunt characteristics. In Sec. V B, discuss experimental results from literature and develop a model for the physical origin of shunt paths for all three thin film cell types. We test these hypotheses in Sec. V C using detailed simulations, and show that the SCL model accounts for all features of shunt current. Section VI concludes the article with a discussion of the implications of this new understanding of shunt leakage in thin film solar cells.

II. METHODS

A. Cell fabrication

The a-Si:H p-i-n solar cells were prepared via plasma-enhanced chemical vapor deposition on fluorinated tin oxide coated glass. The layer structure of the cell [Fig. 2(a)] has SnO_2:F (FTO) as the p contact and ZnO:Al (AZO) as the n contact. The thicknesses of the p, i, and n a-Si:H layers were 10 nm, 250 nm, and 20 nm, respectively. The cell area is 0.5 cm^2. The BHJ OPV cells were prepared via spin-casting poly(3,4-ethylenedioxythiophene) poly(styrenesulfonate) (PEDOT:PSS) onto a tin-doped indium oxide (ITO) substrate. Subsequently, a dicholorobenzene (DCB) solution of poly(3-hexylthiophene) (P3HT) and the fullerene derivative [6,6]-phenyl-C_{61} butyric acid methyl ester (PCBM) was deposited via spin-casting, followed by annealing and then thermal evaporation of LiF and Al cathode layers. A schematic of the materials and layer thicknesses is shown in Fig. 2(b). The cell area is 0.06 cm^2. The details of the fabrication process for BHJ OPV cells have been previously reported.[26] The CIGS cells were fabricated by selenization of $Cu(In,Ga)S_2$ nanocrystals with Mo as the back contact and CdS/ZnO buffer layers on the top, producing the structure

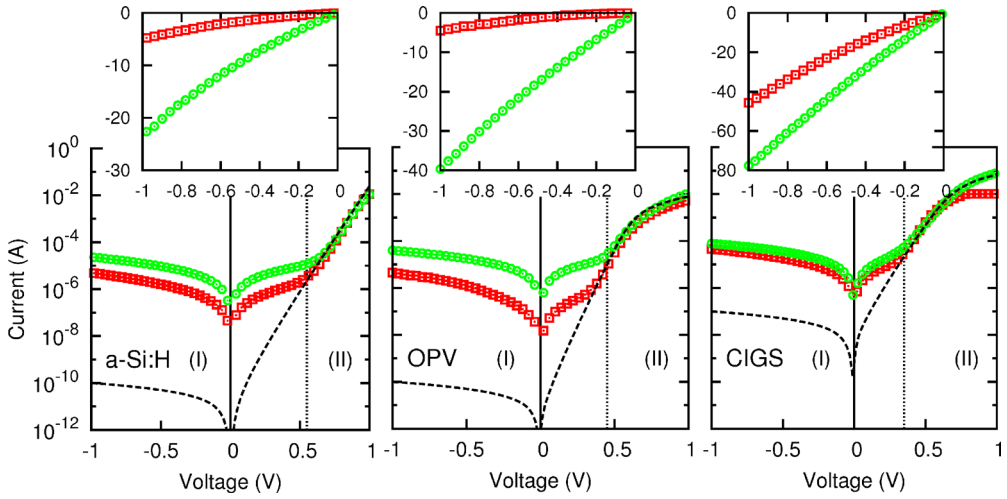

FIG. 3. (Color online) Experimental dark IV characteristics of two samples each (squares and circles) of the three solar cell technologies. Note the similar features, showing an exponential forward current at high forward biases [$V > \sim 0.4-0.5$ V denoted region (II)], and the shunt leakage component at low forward and reverse biases [$V < \sim 0.4-0.5$ V denoted region (I)]. The insets show the reverse current (in microampere) of the two samples, on a linear scale, revealing the nonlinear voltage dependence of the shunt leakage.

shown in Fig. 2(c). The cell area is 0.51 cm^2. The details of the fabrication methods for these cells have been previously reported.[27]

B. Simulations

Ideal solar cell structures are based on a junction formed by two materials with different work functions, band gaps, and/or doping levels, much like a conventional p-n junction diode. A modeling and simulation approach similar to that used for modeling p-n diodes has, therefore, been applied for simulating the exponential diode current (I_d) in all three PV technologies considered.[17,28–32] We apply self-consistent numerical solutions of Poisson and continuity equations for simulating the ideal solar cell structures (i.e., without the parasitic shunt current) of the three thin-film cell types. All simulations were performed using Taurus Medici™ TCAD software. Detailed materials parameters including band-discontinuity, band-tail states, defect levels, capture cross-sections, mobilities, and their temperature activations, for a-Si:H,[33] CIGS,[31] and OPV materials[17] were taken from literature. We then used the same materials parameters for simulating the shunt current (I_{sh}) separately, using the model developed in this paper.

III. MEASUREMENTS AND OBSERVATIONS

We begin by comparing the qualitative features of the room temperature dark current (I_{dark}) for the three cell types. Figure 3 shows the room temperature dark characteristics of two nominally identical samples (squares and circles) of each PV technology. Note that for all three figures, we can identify two distinct regions in the IV curves. The region marked (II) is the high forward bias part (typically $V > \sim 0.4-0.5$), where the two IV curves (squares and circles) overlap for all cell types. This current in region (II) exhibits exponential diode characteristics ($I_d \propto e^{qV/nk_BT}$). This diode current is attributed to the activated carrier transport across a built-in potential barrier. The exact nature and magnitude of this exponential diode current is dependent upon the structural and materials properties of the solar cell. Significant simulation and modeling efforts have been devoted to understanding the nature of transport phenomena of this diode current (I_d) in these different PV technologies.[31,34,35] In an equivalent circuit picture [Fig. 1(b)], these effects are typically captured in the saturation current I_0 and ideality factor n [Eq. (1)]. Also, the current roll-off at high biases is determined by a series resistance R_s based on Eq. (1).

At lower voltages [typically $V < \sim 0.4-0.5$, region (I) in Fig. 3], on the other hand, the current values are very different for these nominally identical devices over all three cell types (compare squares and circles in Fig. 3). Additionally, in this region the current is much greater than what is expected from the ideal, activated diode solar cell model (dashed line in Fig. 3). This excess current at low biases is called the shunt leakage current (I_{sh}). The variability in shunt current (Fig. 3) for nominally identical samples is typical for thin-film solar cells. The shunt current exhibits a different temperature dependence compared to the diode current component (I_d) for each of the three cell types. As shown in Fig. 4, the shunt current [$V < \sim 0.4$ range, labeled region (I) in Fig. 4] increases by a relatively small factor ($\sim$5x) over a large temperature range ($\sim$100 K). In contrast, the exponential diode current in high forward bias regime [$V > \sim 0.4-0.5$, labeled region (II) in Fig. 4], increases significantly by $\sim$300–500x over the same temperature range. The exponential temperature dependence of the diode current (I_d) is consistent with the junction dominated active transport mechanism in an ideal solar cell structure, and its activation energy is determined by the transport phenomena and materials properties of the cell type.

It is common practice to use a constant shunt resistance (R_{sh}) according to Eq. (1) to fit the shunt current part [Fig. 1(b)]. While this usually provides a satisfactory looking fit in the forward bias regime, the approach has several problems. First, there is a large fluctuation in shunt current magnitude from device to device; this typically means that a different

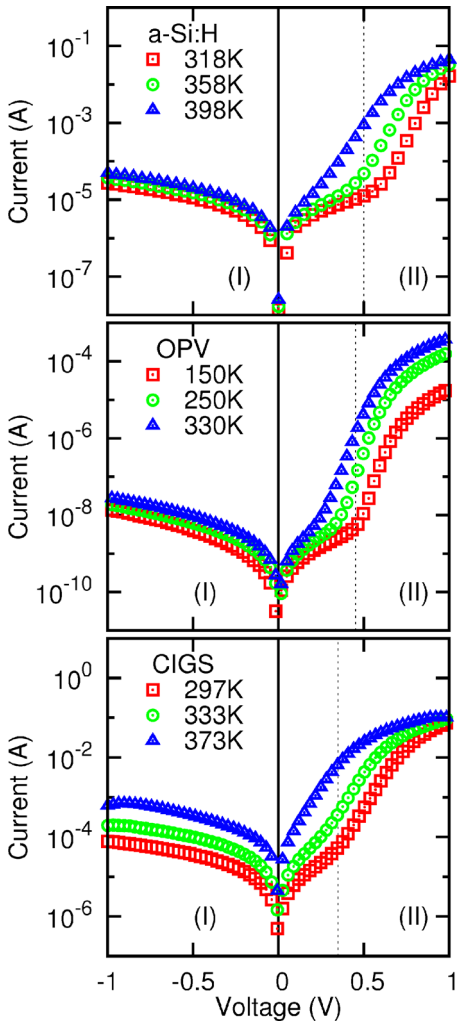

FIG. 4. (Color online) Temperature dependent dark IV characteristics of the three PV technologies over about a 100 °C range, showing the distinct temperature dependence of current in regions (I) and (II) corresponding to shunt and diode dominated regions, respectively.

R_{sh} value must be used for each data set. The other parameters in Eq. (1) (I_0, n, and R_s), on the other hand, typically have consistent values for a given cell type. Furthermore, unlike R_{sh}, the parameters I_0, n, and R_s have clear physical interpretations based on materials and device properties, and these can be reproduced quite well using device level simulations. The fitted shunt resistance value, however, often varies by 2–3 orders of magnitude for cells of the same type, even when they are fabricated under nominally identical conditions.[8] Additionally, the temperature dependence of the diode current (I_d) behavior is consistent with the theoretical predictions using self-consistent simulations. On the other hand, to account for the temperature dependence of the shunt current, an additional fitting parameter in the form of shunt resistance temperature coefficient is needed. Therefore, this traditional shunt resistance value has no correlation with the materials properties or the solar cell structure of the thin-film solar cells discussed here, and a new model is clearly needed to account for the observed shunt current behavior.

Most significantly, note that the shunt current is symmetric around $V=0$ [$|I_{sh}(V_0)| \approx |I_{sh}(-V_0)|$ in Fig. 3, region (I)] for all three cell types. This means that any shunt resistor used to fit the forward characteristics must be able to simultaneously model the reverse current. A closer look at the reverse current, however, reveals that it has distinctly nonlinear voltage dependence [see inset Fig. 3 showing the reverse currents (in microampere) of the same two cells on linear scale]. In fact, we find that the reverse current has power law voltage dependence ($I_{sh} \propto |V|^{\beta}$) with power exponent $\beta = \sim 1.5-2.5$ for all three cell types. This means that an Ohmic shunt is inadequate assumption to account for the reverse current behavior. The origin of this non-Ohmic shunt is discussed in Sec. VI. However, the foregoing discussion of the key electrical features of I_{sh} (in particular voltage symmetry) provides useful insights for device characterization, as discussed below.

IV. DISCUSSION

A. Technological implications

A clear and consistent understanding of the shunt current mechanism is important for identifying its source and removing or reducing it. This will be important for controlling production variability, module efficiency, and yield improvement. Additionally, at the single cell level, the identification and modeling of the shunt current has important consequences for parameter extraction and device and materials characterization. For example, failure to account for this nonlinear shunt current can lead to incorrect parameter extraction from dark current data. This may result in extracted ideality factors that are larger than the actual values, often larger than 2 (which cannot be accounted for by classical diode models). Another issue arises with the studies of parametric degradation (e.g., light-induced degradation in a-Si:H cells). In some of these studies, the change in dark current is monitored to assess the degradation phenomenon. A failure to isolate the actual device current by removing the shunt contribution can lead to incorrect parameter extraction. We now show that based on the analysis presented earlier, one can use a simple subtraction scheme to remove the shunt leakage current (I_{sh}) from measured forward dark current ($I_{\mathrm{dark},f}$).

B. "Cleaning" the forward current

Figure 5 shows the absolute value IV plots (i.e., $|I|$ vs $|V|$) for two samples of each cell type (squares and circles) where the forward and reverse currents overlap for $|V| < \sim 0.4-0.5$ V. This result is expected, owing to the symmetry of the shunt current about $V=0$. We can utilize this symmetry, by removing the shunt component of the forward current. We have seen that the measured forward current ($I_{\mathrm{dark},f}$) is a sum of the exponential ideal diode current component ($I_{d,f}$) and the shunt leakage current [$I_{sh,f}$; Eq. (1)]. In order to determine the actual exponential diode current it is necessary to subtract out the shunt current, i.e., $I_{d,f}=I_{\mathrm{dark},f}-I_{sh,f}$. Now, we can use the symmetry of the shunt current ($|I_{sh,f}|=|I_{sh,r}|$) to determine the exponential diode forward current by simply subtracting the absolute value of the reverse current from the forward current ($I_{d,f}=I_{\mathrm{dark},f}-|I_{sh,r}|$). As shown in Fig. 5, the 'cleaned' forward current thus obtained (pluses and crosses), follows the expected exponential diode current (dashed lines). This cleaned forward current is consistent

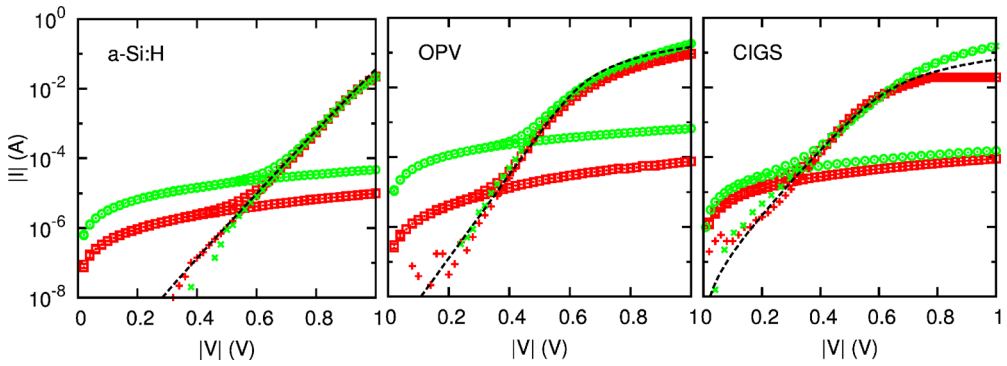

FIG. 5. (Color online) Experimental dark current plotted in absolute value terms; i.e., $|I|$ vs $|V|$, for two samples (shown as squares and circles) each from the three PV technologies discussed, highlighting the voltage symmetry in the shut current (I_{sh}) dominated regime. The "cleaned" current (pluses and crosses) is much closer to the diode model (dashed line).

with the simulations of the idealized solar cell structure and follows the exponential current relation ($I_d \propto e^{qV/nk_BT}$). The noise at the lower current values in this cleaned IV reflects the limitations of the measurement instruments.

This simple subtraction scheme further reinforces the idea that these variable leakage currents are indeed parasitic; and to determine the actual dark characteristics of the solar cell, we must remove the shunt component. Furthermore, this provides a useful tool for cleaning the dark current data, thereby ensuring that the characterization of materials properties through dark IV is not contaminated by parasitic shunt currents. This dispenses with the need to assume an arbitrary shunt resistor for fitting the data, which is an incorrect assumption and potentially introduces errors in extracting other parameter values (I_0, n, and R_s).

V. MODELING

A. SCL current model for I_{sh}

The above discussion identifies the problems of assuming an arbitrary shunt resistance to account for the shunt current in three distinct PV technologies. The intriguing aspect is that even though the shunt current is not resistive, its qualitative features are remarkably similar for all three cell types. This similarity in electrical characteristics, across these very different PV technologies, suggests a possible universal conduction mechanism for shunt current. Such a model will not only provide a consistent explanation of the phenomenon, but also would be able to correlate the shunt conduction to basic materials properties.

In general, any universal model of the shunt leakage must be able to explain all the electrical features of I_{sh} simultaneously for all three cell types. More specifically, the model must account for the weak voltage dependence and weak temperature dependence of the shunt current. A review of the common conduction mechanisms in junction devices shows that almost all of them either have exponential voltage dependence (e.g., Fowler–Nordheim tunneling, thermionic emission), exponential temperature dependence (e.g., Poole–Frenkel effect), or both (e.g., minority carrier injection).[36] Additionally, all these carrier injection and/or tunneling dominated transport mechanisms have rectifying characteristics and cannot account for the symmetry observed for the shunt leakage. The most likely candidate, which might capture both the temperature and voltage dependence features, is a SCL current, as discussed below.

In general, SCL current (I_{SCL}) is not expected in asymmetric structures of solar cells with built-in potentials. It is typically observed in semiconductors with symmetric contacts that inject only one carrier (e.g., a p-i-p or n-i-n structure, or MIM structure with $\phi_1 = \phi_2$) and where the fixed charges inside the semiconductor are negligible compared to the injected charge (e.g., intrinsic semiconductors), as shown in the schematic in Fig. 6.[37] Under these conditions, the space charge density inside the semiconductor is determined by the injected carriers, resulting in symmetric, power law voltage dependence. For example, in the idealized structure shown in Fig. 6, the work functions of the two contacts ensure that only holes can flow in and out easily, and the barrier for electrons is very high. Thus, the entire current is due to hole flux. Assuming an ideal trap-free semiconductor, we can derive the expression for SCL current analytically for the metal-semiconductor-metal (MSM) structure shown in Fig. 6, yielding the following expression for SCL current (I_{SCL}):

$$I_{SCL} = \mathrm{sgn}(V) A \frac{9\varepsilon\mu_c}{8L^3}|V|^2, \tag{2}$$

where A is device area and "sgn" is the sign function, L is the length of semiconductor region, ε is the dielectric constant of the semiconductor, and μ_c is the effective mobility of the injected carrier (holes in the case of schematic shown in Fig.

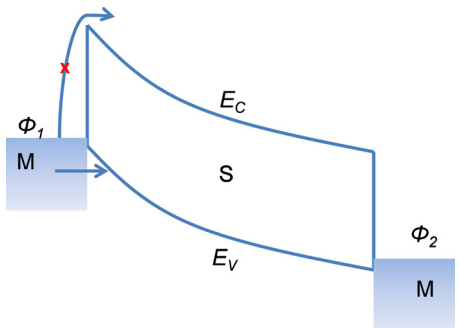

FIG. 6. (Color online) Schematic and band diagram of a MSM structure, showing SCL transport. Both metal work functions ($\phi_1 \approx \phi_2$) ensure that holes are injected preferentially into the semiconductor.

6). This equation, describing the SCL current in an ideal, trap-free semiconductor is known as the Mott–Gurney law.[38] Although this equation describes an ideal trap-free semiconductor, a close examination of Eq. (2) clearly highlights the key features of the SCL conduction mechanism. In addition to the symmetry of the current about $V=0$, we can see the power law voltage dependence ($I_{sh} \propto |V|^{\beta}$). Also, note that the only temperature-dependent term in Eq. (2) is the mobility (μ_c), which is typically a weak function of temperature.[36] This demonstrates that at least qualitatively, the SCL current mechanism can capture all three electrical characteristics of shunt leakage current (I_{sh}) discussed earlier.

The correspondence between shunt current and SCL can be made more precise. In materials with significant trap densities inside the band gap, the SCL current expression has been generalized as:[39,40]

$$I_{\mathrm{SCL}} = \mathrm{sgn}(V) q A \mu_c(\gamma) \frac{|V|^{\gamma+1}}{L^{2\gamma+1}}, \tag{3}$$

where μ_c is the effective carrier mobility as a function of the parameter γ, which in turn depends on the exact nature of trap distribution inside the band gap. Notice that the equation retains its general power law form, and the qualitative features of voltage and temperature dependence remain the same. Depending on the trap distributions and/or contributions from interface trap states, we might have different values for parameter γ, resulting in different power exponents β for different cells (note $\beta=\gamma+1>1$).

The parameter γ is sensitive to the trap distribution inside the semiconductor band gap. Due to this, SCL current is often used to characterize the material properties in semiconductors. In a-Si:H for example, SCL current through n^+-i-n^+ diodes has been used to study the trap distributions.[41,42] For organic polymers as well, recent studies have explored trap dominated SCL current through symmetric structures.[43,44] SCL current has also been observed in CIGS solar cells,[45] and it was suggested as a possible mechanism for the reverse current.[46] However, in Ref. 46 the authors assume this SCL reverse current to be an intrinsic bulk device feature and fail to identify the parasitic nature of this current component.

B. Physical origin

In the previous section, we have seen that a phenomenological SCL current can account for all qualitative features of shunt conduction in the three cell types evaluated here. Beyond the similar electrical characteristics of shunt currents, the statistical and spatial distribution of shunts also exhibits certain common features. In the literature there is considerable evidence from thermography[47,48] and luminescence[49] experiments demonstrating the localized nature of dark current conduction. Moreover, this localized conduction has also been correlated with the random shunt currents in the solar cell.[49] These localized shunts arise primarily because in these cells, thin films of material (~100 nm) must be deposited over large areas (~cm^2) using low temperature processes. This means that any small variation in substrate surface, dust particles, or any other small localized materials property fluctuation can create possible shunt paths at those locations.

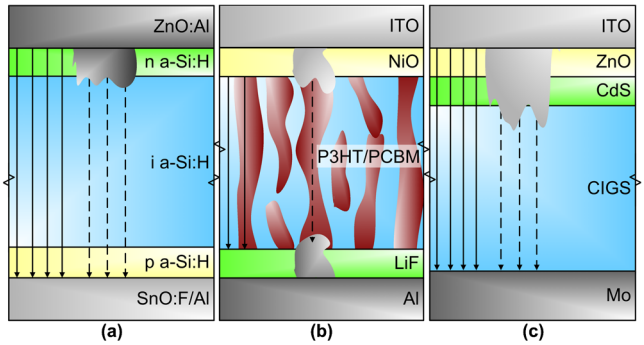

FIG. 7. (Color online) Schematics showing the possible localized shunt structures in (a) a-Si:H cells, (b) OPV cells, and (c) CIGS cells. The dashed lines show the SCL shunt leakage current (I_{sh}) through these structures, which are in parallel to the ideal exponential diode current I_d (solid lines).

Despite these similarities in electrical characteristics, the exact nature of shunt path responsible for an SCL current is expected to be quite different in each PV technology, depending on the cell structure and the materials used. Below we propose mechanisms based on the characterization presented earlier and evidence from the literature, focusing on each PV technology separately.

For a-Si:H p-i-n solar cells, the p and n layers are only ~10 nm thick each. This means that substrate roughness, local doping inhomogeneities, or metal/contact material diffusion into a-Si:H can create a structure which might result in a SCL shunt [see the schematic in Fig. 7(a)]. The most likely way such a shunt path can form, is through a localized Al incursion into the n layer from the top AZO contact. Al is known to diffuse into a-Si:H matrix at high temperatures, which can eventually destroy the n-i junction in p-i-n solar cells.[50] This Al can counter-dope a-Si:H as p-type[51] and induce crystallization.[52] We propose that during deposition of the AZO layer, local variations in deposition conditions such as temperature, microvoids in a-Si:H, etc. can cause Al incursions. This could result in the counter-doping, resulting in formation of localized symmetric a p-i-p structures instead of the ideal p-i-n. Evidence from a-Si:H-based resistive switching memories also supports this Al incursion hypothesis.[53,54] This evidence is especially useful in understanding the phenomenon of shunt busting/curing observed in a-Si:H cells.[8] Shunt busting involves applying a reverse bias to the cell for a certain period of time which results in the shunt current switching to a lower value. There is no clear explanation in the literature for this behavior, however, the shunt picture proposed here, involving metal incursion inside a-Si:H, can explain this observation. It is very likely that during shunt busting, the metal diffuses out of the a-Si:H layer resulting in disruption of the SCL current path (similar to a reset transition in a resistive memory).

In case of OPVs, the solar cell structure is quite complex because the junction is formed by the interpenetrating P3HT:PCBM BHJ matrix. However, shunts can also develop in these systems if the contact materials form complexes at localized points or nonuniformity in interfacial layers is present [see schematic in Fig. 7(b)]. These conditions can result in local variations in contact work functions, resulting in single carrier injection, which will cause a SCL current to

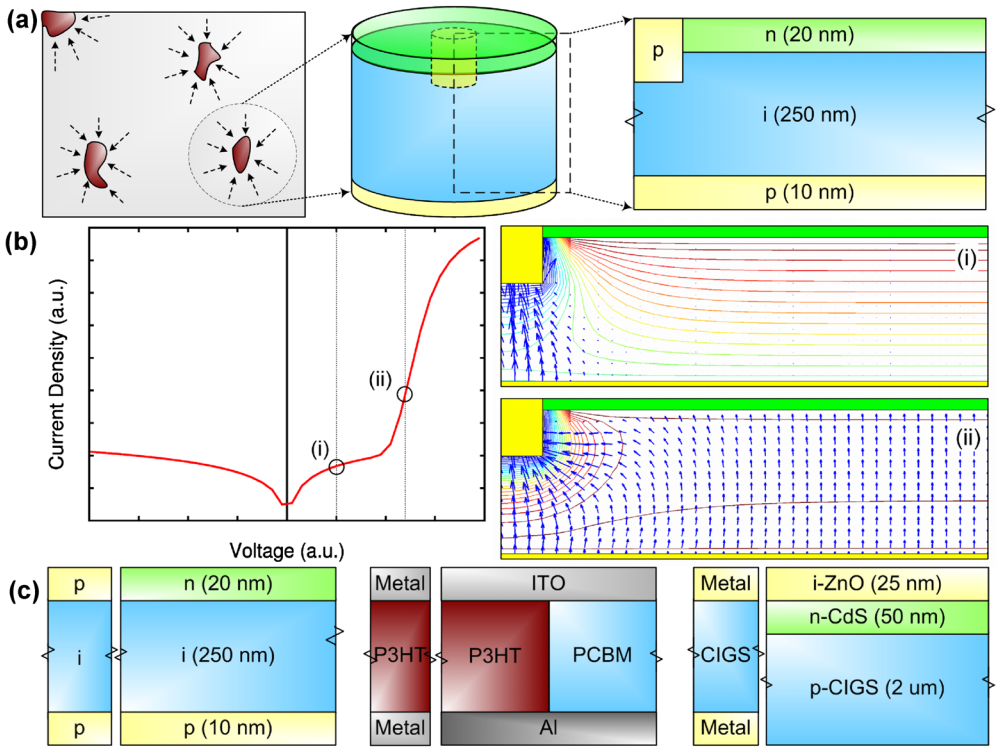

FIG. 8. (Color online) (a) Schematics showing the top view of a solar cell surface with localized shunts. A cylinder is drawn around the shunt region (shown for an a-Si:H p-i-n solar cell) with the shunt formed due to Al incursion. A 2D simulation structure (formed by taking a vertical cut), simulated using cylindrical coordinates, with the p-i-p region in the middle forming the shunt. (b) The dark IV obtained from the 2D simulation of the structure in part (a), reproduces the features of shunt conduction. The quiver (current density) and contour plots (potential), corresponding to the shunt dominated regime [green vertical line denoted by (i)], and the diode dominated regime (blue vertical line denoted by (ii)), showing the localization of dark current at low biases, resulting in a shunt-dominated region. (c) Simplified 1D schematics of the shunt and the idealized solar cells, used for simulating the shunt and device IV separately.

flow. Resistive switching memories similar to a-Si:H have been demonstrated using Al and organic materials such as PEDOT:PSS (Ref. 55) or Cu:TCNQ.[56] Interestingly, in their OFF state, these memories exhibit a symmetric non-Ohmic current similar to the shunt in OPV cells. Note that PEDOT:PSS is commonly used as an interfacial layer in organic BHJ solar cells,[26] and we suspect it, as well as substrate defects, may be involved in the formation of shunt paths.

Finally, in CIGS cells the situation is slightly different since they are not as thin as a-Si:H or OPV cells (CIGS layer thicknesses $\sim 1.5-2.0\ \mu$m). However, the buffer and window layers in these cells (ZnO/CdS) are very thin ($\sim 25-50$ nm). This means that a diffusion of contact metal through ZnO/CdS is possible at localized places, or due to presence of pinholes in these thin layers the usual built-in potential might be missing in certain localized regions [see schematic in Fig. 7(c)]. This localized parasitic structure could result in a SCL current. However, unlike the a-Si:H and OPV cases, where the semiconductor layer is intrinsic, the CIGS layer is doped p-type. This would typically not result in a SCL current. However, due to nonuniformity of electronic properties in CIGS layer (e.g., presence of crystal nanodomains,[57] percolating dislocations or grain boundaries[7] etc.), certain regions may behave as intrinsic material, which can result in SCL shunt current.

Although further experimental work is needed to ascertain the exact nature of the localized shunt path formation in these technologies, we show that the indirect experimental evidence discussed above allows us to reproduce the electrical characteristics of shunt conduction in all three solar cell types using simulation. Based on the above discussion, we can make the modeling assumption that shunts arise at certain locations where both contacts can inject only one of the carriers (electrons or holes) into the intrinsic layer, instead of the ideal diode like conduction. We show that under these assumptions, we can simulate the shunt and ideal device structures separately, and these simulations can reproduce the observed characteristics in a coherent manner.

C. Simulations

We have seen above that the qualitative features of the shunt current (I_{sh}) are best described by a SCL current model. Furthermore, from the previous discussion, we can explore the proposed shunt paths using self-consistent numerical simulations. As apparent from the earlier discussion, the shunt paths are localized structures distributed randomly across the solar cell surface [Fig. 8(a)]. We can consider a cylindrical region around one of them in order to simulate the effects of these local shunts. For this we simulate a vertical cut of such a cylindrical region and simulate the two-dimensional (2D) structure in cylindrical coordinates [shown in Fig. 8(a) for a p-i-n solar cell with middle region forming a p-i-p shunt due to Al incursion]. Figure 8(b) shows the dark IV response obtained from this 2D simulation. We see that this simulation readily reproduces the qualitative features of

the dark current over the entire voltage range. This IV curve can be understood by examining the quiver plots in Fig. 8(b). At lower biases [vertical dotted line marked (i) in Fig. 8(b)], the current is dominated by holes flowing through the p-i-p shunt region since the barrier for holes is very small there [see contours in Fig. 8(b)(i)]. At higher biases [vertical dotted line marked (ii) in Fig. 8(b)(i)] the diode current through the bulk p-i-n region dominates, and the current flow is essentially uniform. This 2D simulation shows that the effect of a parasitic shunt is highly localized and does not affect the potential profile (hence the current) in other regions; this is also apparent from the quiver plot in Fig. 8(b)(ii). This approach allows us to simulate the shunt and device characteristics separately using a one-dimensional (1D) idealized structure and then to add them together [i.e., $I_{\text{dark}}=J_dA_d+J_{sh}A_{sh}$, where A_d is the device (diode) area and shunt area A_{sh} is used as a fitting parameter].

In the case of a-Si:H solar cells, we simulate the shunt using a p-i-p a-Si:H structure in parallel with the ideal p-i-n device. As shown in the first schematic in Fig. 8(c), we can simulate these two structures separately. For simulating organic BHJ OPV cells, the complex interpenetrating structure was simplified to the parallel combination of P3HT and PCBM between two metal contacts. It has been shown that this approximation yields satisfactory results for dark current calculations.[17] In these cells, the shunt may be formed by either of the active materials, which create the percolating path close to the area of local nonuniformity. We simulate this shunt using a M-(P3HT)-M structure [second schematic in Fig. 8(c)]. In CIGS cells, the shunt is assumed to be a M-(intrinsic CIGS)-M in parallel with the ideal CdS/CIGS solar cell structure [right schematic, Fig. 8(c)]. We postulate that these local nonuniformities ensure a single carrier injection to the shunt structure, possibly due to a metal/semiconductor complex formation or localized high electric fields. For simulation purposes, we ensure this single carrier injection by keeping the metal work functions in the M/CIGS/M and M/P3HT/M structure close to the valence band.

Figure 9 demonstrates the results of this full simulation for the shunt structures described above (dashed lines) and the ideal devices (solid lines) at three different temperatures. For all three technologies, the sum of these simulated currents is able to match the dark IV at all temperatures. It is important to note that for simulating the ideal solar cell structures the only fitting parameters used were the midgap trap density, contact series resistance, and temperature dependence of the mobilities. The values of these parameters were also within the range reported in literature.[31,33,35] No additional materials parameters were used in simulating the corresponding shunt structures, for any of the three PV technologies. The net shunt area needed for matching the data was about $\sim 10^{-4}$ to $\sim 10^{-6}$ cm^2, which points toward micrometer size nonuniformities on the surface leading to shunt formation. These simulations demonstrate that this model of parasitic SCL shunt current can account for all the characteristic features of the dark IV response, over the entire voltage and temperature range. More importantly, this simulation is able to extract the shunt behavior directly from the materials

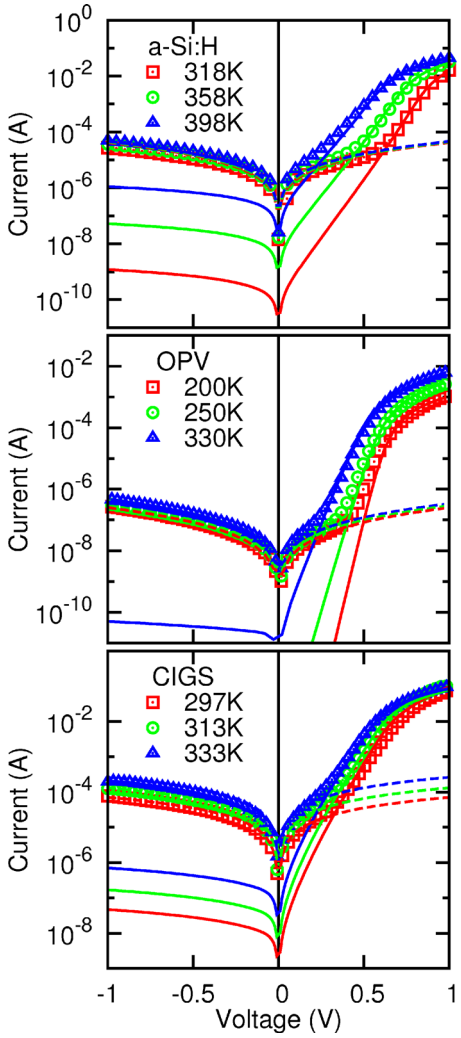

FIG. 9. (Color online) Simulations of the 1D ideal solar cell structures (solid lines) at three different temperatures along with the corresponding shunt structures (dashed lines), showing good agreement with experiment for all PV technologies (symbols). The combination of these two current components explains the entire dark IV response at the indicated temperatures.

parameters of the respective PV technologies. The only assumption involved is of single carrier injection at the local shunt paths. The net shunt area required for fitting the data is also within physical limits and expectations. Thus, these simulations, while necessarily simplified and based on circumstantial evidence, lend quantitative support to the qualitative picture of SCL shunt conduction from Eq. (3). Further experimental studies are needed to ascertain the nature of nonuniformities which lead to single carrier injection at these shunts.

VI. CONCLUSIONS

We have used three significantly different thin-film solar cell technologies to show that the shunt leakage component of the dark current is characterized by universal electrical features. Our measurements on a-Si:H p-i-n cells, organic BHJ photovoltaics, and CIGS solar cells establish the common features of the variable shunt leakage current as voltage symmetry, power law voltage dependence, and weak temperature dependence. We used self-consistent simulations as

well as analytical arguments to show that these features of the leakage current can be understood by a SCL current through microscopic metal-(intrinsic) semiconductor-metal parasitic structures. This model not only explains all observations regarding the leakage current, but is also consistent with a large body of experimental evidence in literature. This SCL current approach of analyzing shunt leakage allows one to bring together the available experimental results and would provide useful guidance for further studies in this area. Finally, we showed how the insights obtained from this characterization lead to a simple subtraction scheme for eliminating the shunt current from measured forward IV. This highlights the importance of removing the shunt current before any reliable characterization or parameter extraction can be done from the measured dark current.

In this work we have presented a generic phenomenological model for analyzing shunt conduction in thin film cells. While the details of shunt formation need to be ascertained through further experimentation, we believe that this work can provide a coherent conceptual framework for understanding such parasitic conduction in solar cells. For example, we would like to note that this phenomenon of non-Ohmic shunt leakage current is not limited to thin-film solar cells, but has also been observed for a variety of solar cells including crystalline silicon.[18] Based on the apparent similarity of this behavior for all these cells, we believe that the proposed model of SCL current could, in principle, be extended to all solar cells in general. Given the general structure of solar cells and their relatively large areas, the possibility of formation of a parasitic shunt path is quite high. All solar cells involve a combination of thin emitter layer/s ($\sim$10–100 nm) and relatively thick absorber layer ($\sim$1–100 μm), that must be deposited over a large area (approximately square centimeter). This means that a nonuniformity during fabrication (due to residues, surface patterning, etc.), can lead to the metals/ITO coming in direct contact with the absorber layer to form a parasitic MSM structure, resulting in a SCL current.

ACKNOWLEDGMENTS

This work was supported by Applied Materials®, the National Science Foundation, the U.S. DOE-BES Columbia University Energy Frontier Research Center, the U.S. DOE-BES Argonne-Northwestern Solar Energy Research (ANSER), an Energy Frontier Research Center (Award No. DE-SC0001059). J.S. thanks the Link Energy Foundation for a graduate fellowship. The authors gratefully acknowledge Karthik Y. and Professor S. Mahapatra from IIT Bombay for useful discussions, the Birck Nanotechnology Center and Northwestern University NSF MRSEC (Grant No. DMR-0520513) for the characterization facilities, and the Network for Computational Nanotechnology (NCN) for computational resources.

[1]K. L. Chopra, P. D. Paulson, and V. Dutta, Prog. Photovoltaics **12**, 69 (2004).
[2]S. Hegedus, Prog. Photovoltaics **14**, 393 (2006).
[3]M. Green, J. Mater. Sci.: Mater. Electron. **18**, 15 (2007).
[4]M. Despeisse, C. Ballif, A. Feltrin, F. Meillaud, S. Fay, F. J. Haug, D. Domine, M. Python, T. Soderstrom, P. Buehlmann, and G. Bugnon, *Research and Developments in Thin-Film Silicon Photovoltaics* (SPIE, San Diego, CA, 2009), pp. 74090B–15.
[5]B. von Roedern and H. S. Ullal, *The Role of Polycrystalline Thin-Film PV Technologies in Competitive PV Module Markets* (2008), pp. 1–4.
[6]B. Kippelen and J.-L. Bredas, Energy Environ. Sci. **2**, 251 (2009).
[7]A. Virtuani, E. Lotter, M. Powalla, U. Rau, J. H. Werner, and M. Acciarri, J. Appl. Phys. **99**, 014906 (2006).
[8]T. R. Johnson, G. Ganguly, G. S. Wood, and D. E. Carlson, "Investigation of the causes and variation of leakage currents in amorphous silicon p-i-n diodes," in *Amorphous and Nanocrystalline Silicon-Based-Films-2003*, Vol. 762, (Materials Research Society, Warrendale, PA, 2003), pp. 381–386.
[9]T. J. McMahon, T. J. Berniard, and D. S. Albin, J. Appl. Phys. **97**, 054503 (2005).
[10]M. D. Irwin, J. Liu, B. J. Leever, J. D. Servaites, M. C. Hersam, M. F. Durstock, and T. J. Marks, Langmuir **26**, 2584 (2010).
[11]M. Igalson, "Metastable defect distributions in CIGS solar cells and their impact on device efficiency," in *Thin-Film Compound Semiconductor Photovoltaics-2007*, Vol. 1012, (Materials Research Society, Warrendale, PA, 2007), pp. 211–222.
[12]K. R. Lord, M. R. Walters, and J. R. Woodyard, "Investigation of shunt resistances in single-junction a-Si:H alloy solar cells," in *Amorphous Silicon Technology-1994*, Vol. 336 (Materials Research Society, Pittsburgh, PA, 1994), pp. 729–734.
[13]O. Kunz, J. Wong, J. Janssens, J. Bauer, O. Breitenstein, and A. G. Aberle, Prog. Photovoltaics **17**, 35 (2009).
[14]R. Martins, A. Bicho, G. Lavareda, and E. Fortunato, Sol. Energy Mater. Sol. Cells **45**, 1 (1997).
[15]P. Schilinsky, C. Waldauf, J. Hauch, and C. J. Brabec, J. Appl. Phys. **95**, 2816 (2004).
[16]V. D. Mihailetchi, P. W. M. Blom, J. C. Hummelen, and M. T. Rispens, J. Appl. Phys. **94**, 6849 (2003).
[17]P. Kumar, S. C. Jain, V. Kumar, S. Chand, and R. P. Tandon, J. Appl. Phys. **105**, 104507 (2009).
[18]O. Breitenstein, J. P. Rakotoniaina, M. H. A. Rifai, and M. Werner, Prog. Photovoltaics **12**, 529 (2004).
[19]M. C. Alonso-García and J. M. Ruíz, Sol. Energy Mater. Sol. Cells **90**, 1105 (2006).
[20]V. G. Karpov, A. D. Compaan, and D. Shvydka, Appl. Phys. Lett. **80**, 4256 (2002).
[21]J. Pallarès, R. Cabre, L. F. Marsal, and R. E. I. Schropp, J. Appl. Phys. **100**, 084513 (2006).
[22]B. G. Yacobi, T. J. McMahon, and A. Madan, Sol. Cells **12**, 329 (1984).
[23]M. S. Haque, H. A. Naseem, and W. D. Brown, Sol. Energy Mater. Sol. Cells **41–42**, 543 (1996).
[24]K. Ottoson, Thesis, Uppsala Universitet, 2006.
[25]T. J. McMahon and A. Madan, J. Appl. Phys. **57**, 5302 (1985).
[26]M. D. Irwin, B. Buchholz, A. W. Hains, R. P. H. Chang, and T. J. Marks, Proc. Natl. Acad. Sci. U.S.A. **105**, 2783 (2008).
[27]Q. Guo, G. M. Ford, H. W. Hillhouse, and R. Agrawal, Nano Lett. **9**, 3060 (2009).
[28]C. van Berkel, M. J. Powell, A. R. Franklin, and I. D. French, J. Appl. Phys. **73**, 5264 (1993).
[29]M. A. Kroon and R. A. C. M. M. van Swaaij, J. Appl. Phys. **90**, 994 (2001).
[30]M. Shah and V. Ganesan, Macromolecules **43**, 543 (2010).
[31]M. Gloeckler, A. L. Fahrenbruch, and J. R. Sites, "Numerical modeling of CIGS and CdTe solar cells: Setting the baseline," in *Proceedings of 3rd World Conference on Photovoltaic Energy Conversion, 2003*, Vol. 1, (WCPEC-3 Organizing Committee, Tokyo Univ. Agriculture & Technology, Tokyo, Koganei 184–8588, Japan, 2003), pp. 491–494.
[32]A. Kanevce, M. Gloeckler, A. O. Pudov, and J. R. Sites, "Conduction-band-offset rule governing J-V distortion in CdS/CI(G)S solar cells," in *Thin-film Compound Semiconductor Photovoltaics*, Vol. 865, (Materials Research Society, Warrendale, PA, 2005), pp. 221–226.
[33]S. S. Hegedus and A. Luque, *Handbook of Photovoltaic Science and Engineering* (Wiley, New York, 2003).
[34]H. Matsuura, A. Matsuda, H. Okushi, and K. Tanaka, J. Appl. Phys. **58**, 1578 (1985).
[35]L. J. A. Koster, E. C. P. Smits, V. D. Mihailetchi, and P. W. M. Blom, Phys. Rev. B **72**, 085205 (2005).
[36]S. M. Sze and K. K. Ng, *Physics of Semiconductor Devices* (Wiley, New York, 2007).
[37]H. Y. Fan, Phys. Rev. **74**, 1505 (1948).

[38]N. F. Mott and R. W. Gurney, *Electronic Processes in Ionic Crystals* (Dover, New York, 1964).
[39]A. Rose, Phys. Rev. **97**, 1538 (1955).
[40]W. Hwang and K. C. Kao, Solid-State Electron. **15**, 523 (1972).
[41]I. Solomon, R. Benferhat, and H. Tran-Quoc, Phys. Rev. B **30**, 3422 (1984).
[42]F. Schauer and O. Zmeskal, J. Non-Cryst. Solids **164–166**, 537 (1993).
[43]G. Paasch and S. Scheinert, J. Appl. Phys. **106**, 084502 (2009).
[44]M. M. Mandoc, B. de Boer, G. Paasch, and P. W. M. Blom, Phys. Rev. B **75**, 193202 (2007).
[45]G. A. Naik and W. A. Anderson, "Current transport mechanisms in $CuIn_{1-x}Ga_xSe_2$ and CIS thin-film solar cells on flexible stainless steel substrates," in *II-VI Compound Semiconductor Photovoltaic Materials Symposium*, Vol. 668 (Materials Research Society, Warrendale, PA, 2001), pp. 3–10.
[46]J.-H. Tan and W. A. Anderson, Sol. Energy Mater. Sol. Cells **77**, 283 (2003).
[47]O. Breitenstein, J. P. Rakotoniaina, S. Neve, M. A. Green, Z. Jianhua, W. Aihua, and G. Hahn, *Lock-in Thermography Investigation of Shunts in Screen-Printed and PERL Solar Cells* (IEEE, Piscataway, NJ, 2002), pp. 430–433.
[48]H. Hoppe, J. Bachmann, B. Muhsin, K.-H. Drue, I. Riedel, G. Gobsch, C. Buerhop-Lutz, C. J. Brabec, and V. Dyakonov, J. Appl. Phys. **107**, 014505 (2010).
[49]K. Bothe, K. Ramspeck, D. Hinken, C. Schinke, J. Schmidt, S. Herlufsen, R. Brendel, J. Bauer, J. M. Wagner, N. Zakharov, and O. Breitenstein, J. Appl. Phys. **106**, 104510 (2009).
[50]M. S. Haque, H. A. Naseem, and W. D. Brown, J. Appl. Phys. **75**, 3928 (1994).
[51]K. V. Krishna, S. Guha, and K. L. Narasimhan, Sol. Cells **4**, 153 (1981).
[52]K. S. Hsu, J. Ou-Yang, L. P. Ren, and G. Z. Pan, Electrochem. Solid-State Lett. **10**, H365 (2007).
[53]J. W. Seo, S. J. Baik, S. J. Kang, Y. H. Hong, J.-H. Yang, L. Fang, and K. S. Lim, Appl. Phys. Lett. **96**, 053504 (2010).
[54]S. H. Jo and W. Lu, Nano Lett. **8**, 392 (2008).
[55]H. Ha and O. Kim, Jpn. J. Appl. Phys. **48**, 04C169 (2009).
[56]T. Kever, U. Bottger, C. Schindler, and R. Waser, Appl. Phys. Lett. **91**, 083506 (2007).
[57]Y. Yan, R. Noufi, K. M. Jones, K. Ramanathan, M. M. Al-Jassim, and B. J. Stanbery, Appl. Phys. Lett. **87**, 121904 (2005).